

$$|\vec{K}_2 - \vec{K}_1| Z | (a^2 - b^2)^{1/2} = \frac{1}{4} K^2 |\vec{K}_1 - \vec{K}_2|^2 \epsilon(t_+, -t_-) . \quad (23)$$

With this fact, the integral over Z becomes trivial and recalling the limits on Z , we finally obtain the expression

$$\frac{4e^2}{\pi} \frac{\eta}{e^{2\pi\eta} - 1} \frac{1}{|\vec{K}_1 - \vec{K}_2|^2} \frac{1}{\epsilon} \frac{1}{(t_+ - t_-)} [(t_+)^m - (t_-)^m] \quad (24)$$

which is identical to the result obtained in Eq. (6). It thus appears rather obvious that the Coulomb t matrix does possess a branch cut along the unitarity axis, contrary to previous assertions. The crucial error in Ref. 2 is that the limit $\delta \rightarrow 0$ was taken in-

correctly to yield the result

$$0 = T(K^2) - T(K^2) \neq \lim [T(K^2 + i\delta) - T(K^2 - i\delta)] \quad \text{as } \delta \rightarrow 0 . \quad (25)$$

We note that $T(K^2)$ does not satisfy the usual unitarity condition owing to the singular factor in the integral in Eq. (7) which gives rise to the extra multiplicative factor shown in Eq. (9). We may obtain a relation which looks more like ordinary unitarity if, like Schwinger,³ we remove a factor $(K^2 - K'^2 + i\delta)^{-m} (2\pi\eta)^{1/2} (e^{2\pi\eta} - 1)^{-1/2}$ from $T(K^2 + i\delta)$ and a similar factor of $(K^2 - K'^2 - i\delta)^m (2\pi\eta)^{1/2} \times (e^{2\pi\eta} - 1)^{1/2}$ from $T(K^2 - i\delta)$ before performing the integral in Eq. (3).

*Work supported in part by the U. S. Air Force Office of Scientific Research, Office of Aerospace Research, under Grant No. 71-1979.

¹C. S. Shastry, L. Kumar, and J. Callaway, Phys.

Rev. A 1, 1137 (1970); C. S. Shastry and A. K. Rajagopal, *ibid.* 2, 781 (1970).

²Gerald L. Nutt, J. Math. Phys. 9, 796 (1968).

³Julian Schwinger, J. Math. Phys. 5, 1606 (1964).

Resonance-Coupling Model for Simple Molecular Reactions*

P. McGuire[†] and C. R. Mueller

Department of Chemistry, Purdue University, Lafayette, Indiana 47907

(Received 23 July 1970; revised manuscript received 9 November 1970)

A strong-coupling model for the simple exchange reaction $A + BC \rightarrow AB + C$ is developed by considering the atom-diatom inelastic problems $A + BC$ and $AB + C$ separately and then introducing coupling between these configurations to allow for reaction. The inelastic systems are developed in the form of self-coupled differential-integral equations and are recoupled by the matrix element over internal states of the resonance energy between the adiabatic surfaces for the separate configurations. The model is applied to the $D + H_2 \rightarrow DH + H$ system and its isotopes in a two-level approximation. At the threshold energy (0.33 eV) for the $D + H_2 \rightarrow DH + H$ system, the calculated reactive total cross section is 1.62 \AA^2 and the DH product is backscattered in the center-of-mass system.

I. INTRODUCTION

Advances in the technique of experimental molecular beams has renewed interest in the microscopic theory of chemical kinetics. In the present paper the dynamics of the simple exchange reaction $A + BC \rightarrow AB + C$ will be considered. To date, the appropriate equations of motion have been considered mainly in the classical case.¹ Quantum mechanically, the dynamics of the reaction may be considered within the framework of scattering theory. Weak-coupling (e.g., distorted wave) models^{2,3} have been developed with the approximation of a linear alignment of A , B , and C ; however they tend to underestimate the observable cross sections.

In these models the scattering amplitude is de-

termined in its integral form for the two-state case. In the present paper, a strong-coupling model from the coupled-differential-equations approach will be investigated also using a two-state approximation. The coupled radial Schrödinger equations will be solved exactly and the R matrix determined numerically.

To begin our model, the relative motion of both configurations $A + BC$ and $AB + C$ is expressed in a common radial coordinate. The self-coupled sets of radial equations for each configuration are developed similar to the atom-diatom inelastic problem.⁴ In Sec. III, coupling is introduced to account for the reactive process. The supposition is made that the self-coupled sets of radial equations for the separate configurations are recoupled by a matrix element over internal states of the resonance en-

ergy between the adiabatic potential surfaces for these configurations.

The recoupled sets of radial equations are reduced to the two-level approximation in Sec. V by neglecting coupling of internal and orbital angular momenta and assuming only one reactant state and one product state. Although this approximation is quite restrictive in general, it may be applied to the $D + H_2 \rightarrow DH + H$ system for which no product excitation is observed.^{5,6} In addition, experimental data^{7,8} is also available for the isotopic systems $H + H \rightarrow H_2 + H$ and $H + D_2 \rightarrow DH + D$.

II. FORMULATION

In the present work, the rearrangement collision $A + BC \rightarrow AB + C$ is considered to be a resonance between the configurations $A + BC$ and $AB + C$. The initial (or reactant) channel a is characterized by its energy, the orbital angular momentum l_a , and the rotational J_a and vibrational state ν_a of the diatom. The product state $AB + C$ is similarly characterized by its energy and quantum numbers l_b , J_b , and ν_b . From Fig. 1 the internal motions of the diatoms BC and AB are described by the vectors \vec{r}_a and \vec{r}_b . The relative motions are described by \vec{R}_a and \vec{R}_b .

Assuming separation of internal and external motions, the wave functions of the separate configurations are written as products

$$\Psi_a(\vec{R}_a, \vec{r}_a) = \psi_a(\vec{R}_a) \Phi_a(\vec{r}_a), \quad (2.1)$$

$$\Psi_b(\vec{R}_b, \vec{r}_b) = \psi_b(\vec{R}_b) \Phi_b(\vec{r}_b),$$

where $\Phi_a(\vec{r}_a)$ and $\Phi_b(\vec{r}_b)$ are the internal-state wave functions to be discussed in detail in Sec. IV.

In these coordinates the respective Hamiltonians are

$$\mathcal{H}_a(\vec{R}_a, \vec{r}_a) = -(\hbar^2/2\mu_a)\nabla_{\vec{R}_a}^2 - (\hbar^2/2\mu_{BC})\nabla_{\vec{r}_a}^2 + V_a(\vec{R}_a, \vec{r}_a), \quad (2.2a)$$

$$\mathcal{H}_b(\vec{R}_b, \vec{r}_b) = -(\hbar^2/2\mu_b)\nabla_{\vec{R}_b}^2 - (\hbar^2/2\mu_{AB})\nabla_{\vec{r}_b}^2 + V_b(\vec{R}_b, \vec{r}_b), \quad (2.2b)$$

where V_a and V_b are the adiabatic eigenvalues of the total electronic Hamiltonians of the separate systems and μ gives the appropriate reduced mass.

To eliminate the need for matching wave functions at artificial boundaries, the functions $\psi_a(\vec{R}_a)$ and $\psi_b(\vec{R}_b)$ must be expressed in a common coordinate. The models of Karplus and Tang³ and of Micha² require the reaction to take place through a linear arrangement of A , B , and C . Thus the coordinate transformation necessary to evaluate the integral form of the scattering amplitude is restricted to this alignment. We shall consider the approximation involved in expressing the initial and final rel-

ative-motion wave functions in the relative coordinate \vec{R} (i. e., the AC vector of Fig. 1). At large distances for the initial configuration, the \vec{r}_a vector may be considered as having constant magnitude which is the bond distance r_{a0} . Averaging over angles of approach, the correct relative-motion wave function (i. e., the plane wave $e^{i\vec{k}_a \cdot \vec{R}_a}$) may be written as a constant multiplying a plane wave in \vec{R} , that is, $Ce^{i\vec{k}_a \cdot \vec{R}}$. The constant C is

$$\sin(\alpha_a k_a r_{a0}) / (\alpha_a k_a r_{a0}),$$

where α_a is the mass ratio $m_B/(m_B + m_C)$. A similar argument with interchange of subscripts holds for the final or product state $AB + C$.

One might then begin by making the assumption the total wave functions are given by

$$\Psi_a(\vec{R}, \vec{r}_a) = \psi_a(\vec{R}) \Phi_a(\vec{r}_a), \quad (2.3a)$$

$$\Psi_b(\vec{R}, \vec{r}_b) = \psi_b(\vec{R}) \Phi_b(\vec{r}_b). \quad (2.3b)$$

The center-of-mass motion may be separated out into the coordinates (\vec{R}, \vec{r}_a) for the configuration $A + BC$ and into (\vec{R}, \vec{r}_b) for $AB + C$. The Hamiltonians for the respective systems are then

$$\mathcal{H}_a(\vec{R}, \vec{r}_a) = -\frac{\hbar^2}{2\mu_{AC}}\nabla_{\vec{R}}^2 - \frac{\hbar^2}{2m_C}\vec{\nabla}_{\vec{R}} \cdot \vec{\nabla}_{\vec{r}_a} - \frac{\hbar^2}{2\mu_{BC}}\nabla_{\vec{r}_a}^2 + V_a(\vec{R}, \vec{r}_a), \quad (2.4a)$$

$$\mathcal{H}_b(\vec{R}, \vec{r}_b) = -\frac{\hbar^2}{2\mu_{AC}}\nabla_{\vec{R}}^2 - \frac{\hbar^2}{2m_A}\vec{\nabla}_{\vec{R}} \cdot \vec{\nabla}_{\vec{r}_b} - \frac{\hbar^2}{2\mu_{AB}}\nabla_{\vec{r}_b}^2 + V_b(\vec{R}, \vec{r}_b), \quad (2.4b)$$

where

$$\mu_{AC} = m_A m_C / (m_A + m_C)$$

and V_a and V_b are the same adiabatic potentials of Eq. (2.2) with the indicated coordinate transformation.

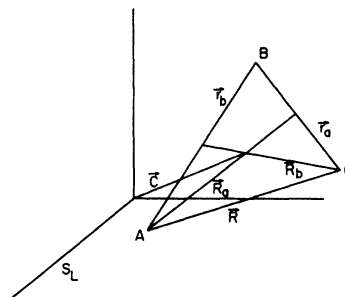


FIG. 1. The position vectors employed in separating the center-of-mass motion \vec{c} defined by the laboratory reference system S_L . Other vectors defined in the text.

The self-coupled sets of differential-integral equations may now be developed to describe the elastic and inelastic features of the separate configurations. Only the configuration $A + BC$ will be considered, the same arguments holding for both systems. The derivation is similar to that for the atom-diatom inelastic problem.⁴ Separating the potential $V_a(\vec{R}, \vec{r}_a)$ into an internal harmonic-oscillator potential $V^{HO}(\gamma_a)$ and an external distortion potential $V_a(\vec{R}, \hat{r}_a)$, and Hamiltonians for the internal motions may be written

$$H_a(\vec{r}_a) = -(\hbar^2/2\mu_{BC})\nabla_{\vec{r}_a}^2 + V^{HO}(\gamma_a) - D_a^0, \quad (2.5)$$

where D_a^0 is the binding energy of the diatom BC .

Expanding $\psi_a(\vec{R})$ in the spherical harmonic function $Y_{lm}(\theta, \phi)$ and the radial functions $X_{al_a}(R)$ and introducing this expression into the Schrödinger equation for the system one obtains

$$\left(\frac{d^2}{dR^2} + \gamma_a \vec{\nabla}_R \cdot \vec{\nabla}_{r_a} - \frac{l_a(l_a+1)}{R^2} - U_a(\vec{R}, \hat{r}_a) + k_a^2 \right) \times \sum_{a'l_a m_a} X_{a'l_a} Y_{l_a m_a}(\theta, \phi) \Phi_a(\vec{r}_a) = 0, \quad (2.6)$$

where $\gamma_a = \mu_{AC}/m_C$ and

$$U_a(\vec{R}, \hat{r}_a) = 2\mu_{AC} V_a(\vec{R}, \hat{r}_a)/\hbar^2.$$

Also, one obtains

$$k_a^2 = 2\mu_{AC}(E_a - \epsilon_a)/\hbar^2,$$

where ϵ_a is the eigenvalue of the internal Hamiltonian.

Multiplying Eq. (2.6) on the left-hand side by $Y_{l_a m_a}^*$ and Φ_a^* , and integrating over $d\Omega$ and $d\vec{r}_a$ generates the coupled set

$$\sum_{a'} \left(\delta_{a'a} \frac{d^2}{dR^2} + F_{a'a}(R) - \delta_{a'a} \frac{l_a(l_a+1)}{R^2} - u_{a'a}(R) + \delta_{a'a} k_a^2 \right) X_{a'l_a}(R) = 0, \quad (2.7)$$

where $\delta_{a'a}$ is the Kronecker δ function and

$$F_{a'a}(R) = \gamma_a \int d\Omega d\vec{r}_a Y_{l_a m_a}^*(\theta, \phi) \Phi_a^*(\vec{r}_a) \times \vec{\nabla}_R \cdot \vec{\nabla}_{r_a} Y_{l_a m_a}(\theta, \phi) \Phi_a(\vec{r}_a). \quad (2.8)$$

Also from Eq. (2.7) we have the self-coupling matrix element

$$u_{a'a}(R) = \int d\Omega d\vec{r}_a Y_{l_a m_a}^*(\theta, \phi) \Phi_a^*(\vec{r}_a) \times U_a(\vec{R}, \hat{r}_a) Y_{l_a m_a}(\theta, \phi) \Phi_a(\vec{r}_a). \quad (2.9)$$

The corresponding self-coupled set of differential-integral equations for the configuration $AB + C$ is

$$\sum_{b'} \left(\delta_{b'b} \frac{d^2}{dR^2} + F_{b'b}(R) - \delta_{b'b} \frac{l_b(l_b+1)}{R^2} - u_{b'b}(R) + \delta_{b'b} k_b^2 \right) X_{b'l_b}(R) = 0, \quad (2.10)$$

where $F_{b'b}$ and $u_{b'b}$ are defined similar to Eqs. (2.8) and (2.9) with the exchange of subscripts. In Sec. III, recoupling between $X_{a'l_a}$ and $X_{b'l_b}$ will be introduced to account for the exchange process.

III. RESONANCE COUPLING

If one begins the investigation of the reactive system $A + BC \rightarrow AB + C$ by treating the entire system collectively, one might make the initial assumption that the total wave function is

$$\Psi_T = \psi_a(\vec{R}_a) \Phi_a(\vec{r}_a) + \psi_b(\vec{R}_b) \Phi_b(\vec{r}_b). \quad (3.1)$$

This leads to a coupling term between the radial wave functions (e.g., X_{al_a} and X_{bl_b}) which is of second order. We shall consider the concept of resonance energy between adiabatic electronic states which will allow us to estimate the coupling in zero order and thus bring the problem to tractable form.

The significance of the resonance energy between adiabatic electronic states is well known from the Landau⁹ and Zener¹⁰ expression for the probability of crossing. A similar situation exists for the exchange reaction $A + BC \rightarrow AB + C$ except that one is now dealing with the crossing of potential energy surfaces.¹¹ The nature of these adiabatic surfaces is shown in Fig. 2(a) from the work of Evans and

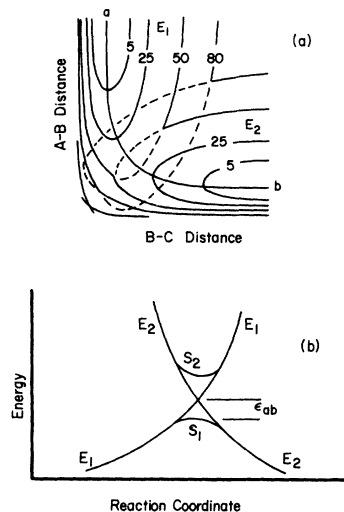


FIG. 2. (a) Schematic representation of the repulsive London surfaces for the linear arrangements of A with BC (E_1) and AB with C (E_2). The line $a-b$ indicates the reaction path and the units are arbitrary. (b) Schematic section along the reaction path $a-b$ from Fig. 2(a). S_1 and S_2 are the surfaces resulting from the introduction of configuration interaction and ϵ_{ab} is the resonance energy.

Polanyi¹² for a collinear symmetric system. By consideration of the interaction of configurations in the region of intersection, the repulsive surfaces E_1 and E_2 split into a smooth lower surface S_1 and a basinlike upper surface S_2 . This effect is observed in Fig. 2(b) where the reaction path is the path of minimum potential.

The resonance energy ϵ_{ab} is a measure of the degree of electron redistribution occurring upon transition from surface E_1 to E_2 . The magnitude and range of ϵ_{ab} are expected to be smaller the more extensive the reorganization of the electronic structure. Thus, for homopolar reactions of the type $D + H_2 \rightarrow DH + H$, the resonance energy will be comparatively large.

Golden¹³ has developed the probability formula for surface crossing from time-dependent perturbation theory. The resonance energy has the same role here as in the Landau-Zener curve-crossing expression used to calculate reaction rates.¹⁴ That is, the greater ϵ_{ab} , the greater the reaction probability. With this property in mind and the fact that the resonance energy is defined in the region where one expects the reaction to occur, we make the supposition that the coupling between the radial wave functions is given by the matrix element over the resonance energy

$$U_{ab}(R) = (2\mu_{AC}/\hbar^2) \int d\Omega d\vec{r}_a Y_{l_a m_a}^*(\theta, \phi) \Phi_a^*(\vec{r}_a) \times \epsilon_{ab}(\vec{R}, \vec{r}_a) Y_{l_b m_b}(\theta, \phi) \Phi_b(\vec{r}_b) . \quad (3.2)$$

Now the position of the coupling between the radial wave functions $X_{a'l'_a}$ and $X_{b'l'_b}$ of Eqs. (2.7) and (2.10) will be determined by the position of the resonance energy.

The self-coupled sets of differential-integral equations from Sec. II may now be recoupled by this resonance coupling term $U_{ab}(R)$ to describe the entire system, giving

$$\sum_{a'} \left(\delta_{a'a} \frac{d^2}{dR^2} + F_{a'a}(R) - \delta_{a'a} \frac{l_a(l_a+1)}{R^2} - u_{a'a}(R) + \delta_{a'a} k_a^2 \right) X_{a'l'_a}(R) = \sum_b U_{ab}(R) X_{b'l'_b}(R) , \quad (3.3a)$$

$$\sum_{b'} \left(\delta_{b'b} \frac{d^2}{dR^2} + F_{b'b}(R) - \delta_{b'b} \frac{l_b(l_b+1)}{R^2} - u_{b'b}(R) + \delta_{b'b} k_b^2 \right) X_{b'l'_b}(R) = \sum_a U_{ba}(R) X_{a'l'_a}(R) . \quad (3.3b)$$

The scattering attributes of the total system are determined by imposing boundary conditions upon $X_{a'l'_a}$ and $X_{b'l'_b}$ and then solving this set of equations to whatever degree of approximation is computationally feasible. We shall consider these boundary conditions within a two-level approximation in Sec. VI.

IV. INTERNAL EIGENFUNCTIONS AND EIGENVALUES

Implicit in the recoupling of Eqs. (3.3a) and (3.3b) is that the total energy of the system be conserved in passing from one configuration to the other. We have that $E_a = E_b$ or

$$\hbar^2 k_a^2 / 2\mu_{AC} + \epsilon_a(\nu_a, J_a) = \hbar^2 k_b^2 / 2\mu_{AC} + \epsilon_b(\nu_b, J_b) . \quad (4.1)$$

Assuming separation of vibrational and rotational motions, the internal wave functions take the well-known form¹⁵

$$\Phi_a(\vec{r}_a) = r_a^{-1} S_{\nu_a}(\xi_a) Y_{J_a M_a}(\theta_a, \phi_a) , \quad (4.2)$$

with $\xi_a = r_a - r_{a0}$. The $Y_{J_a M_a}$ are the spherical harmonics and $S_{\nu_a}(\xi_a)$ is just the simple harmonic-oscillator wave function.

The internal Hamiltonian is

$$H_a(\vec{r}) = -(\hbar^2/2\mu_{BC}) \nabla_{r_a}^2 + \frac{1}{2} \mu_{BC} \omega_a^2 (r_a - r_{a0})^2 - D_a^0 , \quad (4.3)$$

where D_a^0 is the binding energy of BC . The resulting eigenvalue is

$$\epsilon_a(\nu_a, J_a) = h\omega_a(\nu_a + \frac{1}{2}) + \hbar^2 J_a(J_a + 1)/2I_a - D_a^0 , \quad (4.4)$$

where ω_a is the frequency of the oscillator and I_a is the moment of inertia of the diatom BC .

The counterparts to these expressions for the molecule AB are obtained by simple interchange of subscripts. Second-order effects due to the anharmonicity of the harmonic-oscillator potential and the coupling of rotational and vibrational motions have been neglected.

V. TWO-LEVEL APPROXIMATION

As a preliminary test of our model, an approximate calculation on the reactive system $D + H_2 \rightarrow DH + H$ and its isotopes has been performed. As mentioned in the Introduction, experimental scattering data are available for comparison. In addition, the experimental evidence is that the product molecule is not internally excited. This reduces significantly the number of coupled equations which must be considered. The potential energy of these systems is also well characterized by the H_3 semi-empirical surface of Porter and Karplus.¹⁶ The magnitude and position of the resonance energy ϵ_{ab} may be estimated from this potential surface.

To reduce the problem to a two-state system the assumption of spherically symmetric distortion potentials is made. Thus there will be no coupling of internal and external angular momenta. Since it is known that there is no product excitation, this assumption may not be overly restrictive for this system. If we make the additional assumption that the resonance energy is also spherically symmetric, then from the form of the resonance-coupling term $U_{ab}(R)$ we will have $l_a = l_b (= l)$. Spherically symmetric but segmented potentials were employed in the

model by Micha² with the similar condition that $\Delta l = 0$ upon reaction.

The recoupled system of equations is now reduced to the coupled radial equations

$$\left(\frac{d^2}{dR^2} - \frac{l(l+1)}{R^2} - U_{aa}(R) + k_a^2 \right) X_{a1}(R) = U_{ab}(R) X_{b1}(R), \quad (5.1a)$$

$$\left(\frac{d^2}{dR^2} - \frac{l(l+1)}{R^2} - U_{bb}(R) + k_b^2 \right) X_{b1}(R) = U_{ba}(R) X_{a1}(R). \quad (5.1b)$$

For this two-level system then, no inelastic channels are open. The matrix elements U_{aa} and U_{bb} are just the symmetric matrix elements of the external distortion potentials. These potentials were obtained in the relative coordinate R by angular average of the two-body (H, H₂) potential of Tang and Karplus.¹⁷

The Gaussian form $Ae^{-\alpha(R_a - R_c)^2}$ was taken for the resonance energy $\epsilon_{ab}(R_a)$, where R_c is the radial distance in R_a corresponding to the position of the saddle point. From the H₃ surface¹⁶ we set $A = 0.28$ eV, $R_c = 1.2$ Å, and let $\alpha = 36$. The integration of Eq. (3.2) then gave the coupling matrix element $U_{ab}(R)$ which is shown in Fig. 3, along with the $U_{aa}(R)$ potential. For the present system $U_{ab}(R) = U_{ba}(R)$ and $U_{aa}(R) = U_{bb}(R)$. The difference between U_{ab} at its maximum R_m and the matrix element U_{aa} at that point should be proportional to the activation energy of the system. Thus increasing R_m would, in effect, reduce the energy of activation and increase the reactive cross sections.

VI. METHOD OF CALCULATION

With the potentials defined, the two-level equa-

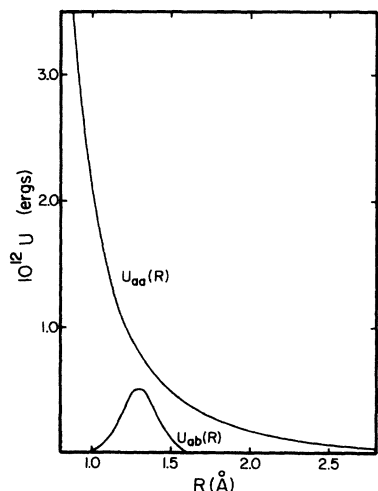


FIG. 3. The matrix-element potential $U_{aa}(R)$ and the spherically symmetric resonance-coupling potential $U_{ab}(R)$.

tions of Sec. V may be solved numerically and the scattering cross sections computed. We have employed the method of deVogelaere¹⁸ which has been applied to the atom-diatom rotationally inelastic problem.⁴ In general, N second-order coupled equations require $2N$ boundary conditions for solution. At the origin we have, for the l th partial wave, $\chi_j' \rightarrow 0$ and asymptotically ($R \rightarrow \infty$) the boundary condition for scattering in terms of the R matrix¹⁹

$$\chi_{j,j'} \rightarrow \delta_{j,j'} \sin(k_j R - \frac{1}{2}l\pi) + (k_j/k_{j'})^{1/2} R_{j,j'} \cos(k_j R - \frac{1}{2}l\pi), \quad (6.1)$$

where j may be either a or b . Most numerical algorithms (including that of deVogelaere) require the derivative of $\chi_j'(R)$ at $R=0$. Taking N linearly independent sets of derivatives at $R=0$ will allow us to generate N independent solution vectors into the asymptotic region. The matrix of initial derivative vectors must be nonsingular in order that the generated solution vectors be linearly independent.⁴

The collection of solution vectors is the solution matrix which may be written²⁰ asymptotically as

$$\underline{\chi}_0 \rightarrow \underline{J}\underline{X} - \underline{N}\underline{Y}, \quad (6.2)$$

where \underline{J} and \underline{N} are the diagonal matrices of the asymptotic forms of the spherical Bessel and Neumann functions for the various channels j . The coefficient matrices \underline{X} and \underline{Y} are constants and may be written in terms of the amplitudes and phase shifts of the numerical solutions. However, the asymptotic boundary condition Eq. (6.1) may be written in the matrix form

$$\underline{\chi} \rightarrow \underline{J} - \underline{N}\underline{k}^{-1/2}\underline{R}\underline{k}^{1/2}, \quad (6.3)$$

where \underline{k} is the diagonal matrix of the wave numbers k_j . And as Gordon²⁰ has shown, the actual phase shifts and amplitudes themselves need not be computed. Instead, the matrices \underline{X} and \underline{Y} are determined by matching the numerical solution matrix $\underline{\chi}_0$ and its derivative $\underline{\chi}'_0$ at large R through the equations

$$\underline{X} = (\underline{J}\underline{N}' - \underline{N}'\underline{J})^{-1}(\underline{N}'\underline{\chi}_0 - \underline{N}\underline{\chi}'_0), \quad (6.4a)$$

$$\underline{Y} = (\underline{J}\underline{N}' - \underline{N}\underline{J}')^{-1}(\underline{J}'\underline{\chi}_0 - \underline{J}\underline{\chi}'_0). \quad (6.4b)$$

Having obtained \underline{X} and \underline{Y} , the \underline{R} matrix is found by comparing Eq. (6.2) with Eq. (6.3) to be

$$\underline{R} = \underline{k}^{1/2}\underline{Y}\underline{X}^{-1}\underline{k}^{-1/2}. \quad (6.5)$$

Having obtained \underline{R} , the unitary and symmetric \underline{S} matrix is given by

$$\underline{S} = (\underline{1} + i\underline{R})(\underline{1} - i\underline{R})^{-1} \quad (6.6)$$

for each partial wave. The elastic and reactive differential cross sections are the sums over partial waves²¹

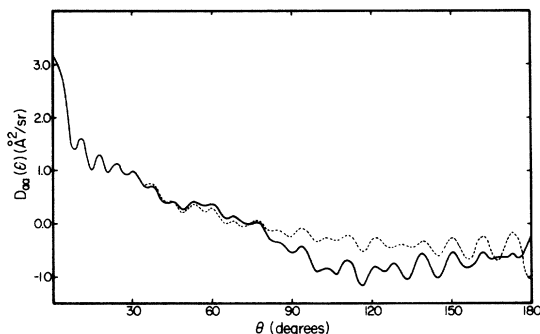


FIG. 4. Elastic differential cross section of D with H_2 at 0.33 eV calculated with (solid line) and without (dotted line) the resonance coupling $U_{ab}(R)$.

$$D_{jj'}(\theta) = \frac{1}{4k_j^2} \left| \sum_{l=0}^{\infty} (2l+1)(S_{jj'}^l - \delta_{jj'}) P_l(\cos\theta) \right|^2. \quad (6.7)$$

The total cross sections are the sums

$$\sigma_{jj'}(k) = \frac{\pi}{k_j^2} \sum_{l=0}^{\infty} (2l+1) |T_{jj'}^l|^2, \quad (6.8)$$

where $T_{jj'}^l = \delta_{jj'} - S_{jj'}^l$.

The deVogelaere algorithm has been programed in FORTRAN IV for the CDC 6500 computer and the numerical solutions checked against analytic solutions for the coupled oscillator.²² The symmetry of the \underline{R} matrix provided a check of the computations. The detailed balance relation from time-reversal invariance²³

$$k_j^2 \sigma_{j'j}^l = k_{j'}^2 \sigma_{jj'}^l, \quad (6.9)$$

was also monitored.

VII. COMPUTATIONAL RESULTS

Using the potentials of Fig. 3, the scattering cross sections have been calculated for the ($\nu_a = 0, J_a = 0$) to ($\nu_b = 0, J_b = 0$) reaction of D + H_2

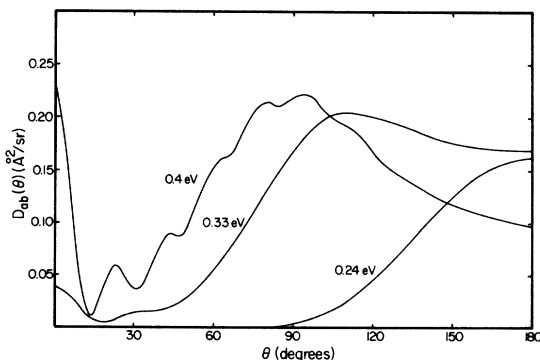


FIG. 5. Reactive differential cross section of the DH product from the D + H_2 collision at various energies.

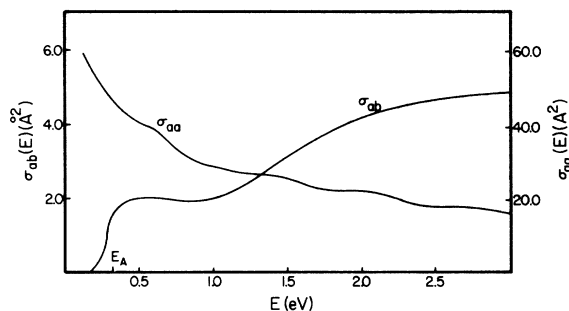


FIG. 6. Elastic σ_{aa} and reactive σ_{ab} total cross section for the D + $H_2 \rightarrow DH + H$ system as a function of energy. E_A is the assumed energy of activation (0.33 eV).

– DH + H and its isotopes. The elastic scattering of D on the diatom H_2 computed at 0.33 eV with and without the coupling term is given in Fig. 4. The effect of coupling is minimal in the forward quadrant while reducing the differential by as much as one-half of a log unit in the back quadrant ($90 - 180^\circ$). The total elastic cross section without coupling (45.7 \AA^2), however, is only slightly greater than that with (45.3 \AA^2).

Figure 5 shows the reactive differential cross section for the DH product from the D + H_2 reaction at three energies. At the assumed²⁴ energy of activation of 0.33 eV, the scattering is predominantly in the back quadrant. The variation of incident energy from subthreshold to superthreshold illustrates an interesting result similar to that observed by Karplus and Tang³ in their weak-coupling model for H + H_2 reactive scattering. They observed a reactive peak of constant magnitude which shifted smoothly from back- to frontscattering while building up a new peak at 180° . We also find a shift in scattering mode with increasing energy but one of a slightly different character. It is found that as the back peak moves forward to the 90° region, a new peak develops at 0° instead of at 180° . This 0° peak is not observed by Karplus and Tang even up to 1.5 eV. In the present work this peak is sharply defined at 0.4 eV with a magnitude that dominates the residual backscattering as the energy is further increased.

The elastic and reactive total cross sections for D + $H_2 \rightarrow DH + H$ are plotted in Fig. 6 as a function of energy. Characteristically, the elastic curve tails off slowly with slight undulations. The reactive curve contrasts with the similar curve from classical trajectory calculations¹ in that our quantum model predicts one large undulation and a considerable amount of tunneling beginning at 0.22 eV.

Another contrast with classical calculations is the probability of reaction as a function of impact parameter b . In Fig. 7 we show the quantum-mechanical counterpart which is the transition matrix

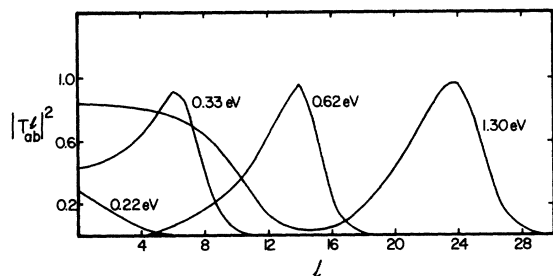


FIG. 7. Reaction probability for the $D+H_2 \rightarrow DH+H$ as a function of orbital angular momentum l for various incident energies.

element squared ($|T_{ab}^l|^2$) as a function of orbital angular momentum l . The classical curve is a monotonically decreasing function with a maximum at $b=0$. From our model (making the correspondence $l=bk_a$) we see, in Fig. 7, that at a given energy, certain l values are highly preferred, while others contribute little to the reaction. It is also noted that at low energies, low l values are preferred, corresponding to "head-on"-type reactive collisions, and at higher energies, high l values are favored which correspond to "stripping" reactions. This explains the shift in the reactive differential cross section from back- to frontscattering.

With the same potentials as above the scattering cross sections for the isotopic systems $H+H_2 \rightarrow H_2+H$ and $H+D_2 \rightarrow DH+D$ have been calculated at 0.33 eV. Considerable confusion exists in both the theoretical and experimental work on the $H+H_2$ system. The theoretical calculations have universally neglected the effect of nuclear symmetry and the experiments have been interpreted on the basis of symmetry factors from an activated complex formulation. We have made these calculations primarily for theoretical comparison and the correspondence with experiments should not be taken

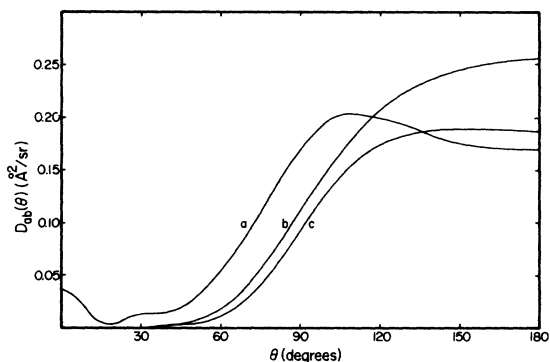


FIG. 8. The reactive differential cross section for the systems a $D+H_2 \rightarrow DH+H$, b $H+H_2 \rightarrow H_2+H$, and c $H+D_2 \rightarrow DH+D$ at 0.33 eV.

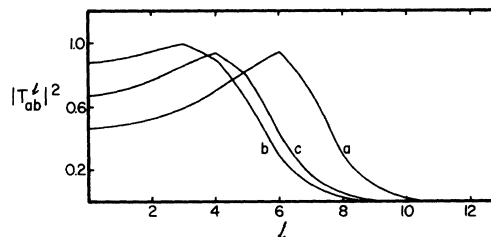


FIG. 9. The reactive probability as a function of orbital angular momentum at 0.33 eV for the systems a $D+H_2 \rightarrow DH+H$, b $H+H_2 \rightarrow H_2+H$, and c $H+D_2 \rightarrow DH+D$.

too seriously. In Fig. 8 the reactive differential cross sections of the three systems (including $D+H_2 \rightarrow DH+H$) are compared. The transition (or reaction) probabilities are given in Fig. 9. It can be seen that the $D+H_2 \rightarrow DH+H$ reaction takes place preferably at higher l values, and is more front scattered. The total reactive cross sections are 1.62 Å², 1.45 Å², and 1.09 Å² for the systems $D+H_2 \rightarrow DH+H$, $H+H_2 \rightarrow H_2+H$, and $H+D_2 \rightarrow DH+D$, respectively. A crude correlation can be made with the experimental rate constants²⁵ at 1000 °K. They are 2.5, 2.2, and 1.2 in units of 10^{-10} cm³/mole sec.

In the present model no consideration has been given to the possible existence of virtual states in the form of long-lived complexes of $(A-B-C)$. Having obtained the S matrix as a function of energy, the delay-time (or lifetime) matrix may be calculated by²⁶

$$(\Delta t)_{jj'} = \text{Re} \left(-i\hbar (S_{jj'})^{-1} \frac{dS_{jj'}}{dE} \right). \quad (7.1)$$

For the reactive collision $D+H_2 \rightarrow DH+H$ at 0.33 eV, at the most probable quantum number ($l=6$), the delay time is $\sim 10^{-14}$ sec which is of the same order as that required for an elastic collision. This justifies the assumption of a direct mechanism for reaction and is consistent with experimental observation.

The experimental differential cross sections^{5,6} for the $D+H_2 \rightarrow DH+H$ system have been transformed to the center-of-mass system²⁷ using an H_2 velocity of 1.12×10^5 cm/sec (most probable for a Maxwellian beam at 100 °K) and a D velocity of 8×10^5 cm/sec. More recent data are available for this system²⁸; however they are qualitatively the same as the original work of Fite.⁶ The original data are compared to the calculated cross section at 0.24 eV in Fig. 10. The data are from a distribution of energies near the threshold for reaction, and since they are relative they have been normalized to the theoretical curve at 180°. At 0.33 eV the computed reactive total cross section is 1.62 Å². Extrapolating the preexponential factor from the kinetic data of Ridley, Schulz, and Le Roy²⁹ to the temperature of the experimental D beam (2800) °K gives a cross section

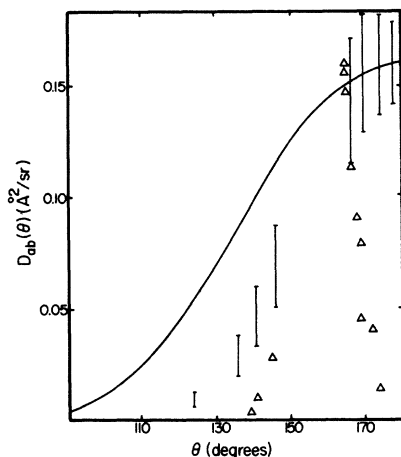


FIG. 10. The solid line is the computed differential cross section at 0.24 eV. The bars are the data of Fite (Ref. 6) and the triangles the data of Datz and Taylor (Ref. 5) transformed to the center-of-mass system.

of $\sim 1.0 \text{ \AA}^2$. The weak-coupling model of Micha² gives a mean cross section which is considerably lower than this ($\sim 0.33 \text{ \AA}^2$).

The absolute elastic total cross section for H on H_2 has been measured by Harrison⁷ to be $\sim 50 \text{ \AA}^2$ at a relative velocity of $9 \times 10^5 \text{ cm/sec}$. For this system, at this velocity, we calculate 46.8 \AA^2 . Our model predicts a reactive total cross section of 1.45 \AA^2 (at 0.33 eV) while the weak-coupling models^{2,3} report values lower by a factor of 10 in the same energy region.

The experimental elastic scattering data⁸ for H upon D_2 have been transformed to the center of mass using the most probable velocity of H at 3000 °K and D_2 at 77 °K. These data along with the calculated curve at 0.33 eV are shown in Fig. 11. The open circles are the originally reported data, while the solid circles are the same data revised as a result of a systematic experimental error.⁸ The computed elastic total cross section is 47.1 \AA^2 while the experimental data are reported as having been normalized to a value of $\sim 50 \text{ \AA}^2$. Even so, the inconsistency still seems to be a matter of a scaling factor. No correction due to the velocity distributions in the beams has been made in converting the data to the center of mass, and this may be an explanation of the difference. However, the elastic scattering of H upon H_2 calculated by Tang and Karplus¹⁷ has been compared to these data in the laboratory system with a similar discrepancy.

From their measurements in the laboratory system, Fite and Brackmann⁸ have estimated the reactive DH product from this system to be backscattered in the center of mass with an absolute value of $0.2\text{--}0.3 \text{ \AA}^2/\text{sr}$. The present model gives a 180° peak of $0.19 \text{ \AA}^2/\text{sr}$ at 0.33 eV and is com-

pletely backscattered. The calculated total cross section for this system is 1.09 \AA^2 while the weak-coupling model of Micha² was again lower than this figure by nearly a factor of 10.

For both systems $\text{D} + \text{H}_2 \rightarrow \text{DH} + \text{H}$ and $\text{H} + \text{D}_2 \rightarrow \text{DH} + \text{H}$ a sharp forward peak begins to build up beyond 0.33 eV. This would correspond to the stripping mode for these systems which has not been observed experimentally. However, the experimental work to date has been predominantly at or below threshold energies. There is also concern that this forward peak may be obscured by impurities (undissociated HD) in the primary beam.

VIII. DISCUSSION

The acceptability of the present model rests largely with the validity of the major assumptions regarding the use of the "common" radial coordinate and the approximation of the coupling with a matrix element of the resonance energy. The coordinate problem is essentially that of the three-body problem in classical mechanics and some approximation must be made to be able to describe the radial motion of both configurations simultaneously. Preaveraging the relative-motion wave functions no doubt destroys the exact dynamics of the exchange process; however, we expect the qualitative features to remain unchanged.

The assumption involving the introduction of the resonance coupling is largely a matter of practicality, although based on a physically acceptable idea. This approximation produces a feasible three-dimensional model, the validity of which might partially be determined by an exact one-dimensional calculation of the total cross section.

The degree of approximation necessary to produce a tractable three-dimensional model is certainly disconcerting from a theoretical point of view. If, however, the model is consistent with observa-

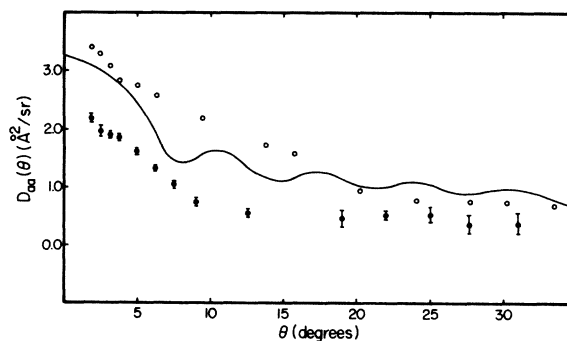


FIG. 11. The solid is the computed elastic differential cross section for H upon D_2 at 0.33 eV. The data are the original (open circles) and the later revised (solid circles with error bars) results of Fite and Brackmann (Ref. 8) transformed to the center-of-mass system.

tion, it is at least partially justified. Our comparison to experiment has been made within the two-state approximation. The lack of coupling is hopefully not overly restrictive for the $D + H_2 \rightarrow DH + H$ system since no product excitation is observed experimentally and also since only ten partial waves contribute significantly to the reactive sections near threshold. Our comparison to experiment in Sec. VII is at least qualitative and in the only two instances of absolute measurements (the H upon H_2 elastic total and the reactive differential for DH from the $H + D_2$ reaction) it is reasonably quantitative. From an experimental point of view the predicted cross sections appear to be reasonable; however, nothing definite may be said until more absolute data are available. By comparison, the models of Micha² and Karplus and Tang³ tend to give extremely low cross sections (in many cases a factor of 10 below our values). Presumably this is a result of the weak-coupling nature of their models.

The observed isotopic effects are an interesting measure of the sensitivity of the model. With the change in reduced masses and dissociation energies, measurable effects are observed in the cross sections. The differential cross sections and the reaction probabilities indicate changes in the dynamics consistent with what one would expect for the re-

spective changes in nuclear masses. In addition, the total reactive cross sections are interrelated in a manner consistent with the observed rate constants for the various isotopes.

The resonance-coupling approximation provides an interesting heuristic study of the relationship between the radial position of reaction and the mode of scattering. This relationship is seen through the transition (or reaction) probability as a function of external angular momentum l . The coupling at small radial distances gave a maximum transition probability at low l values (low-impact parameters, classically) and produced a backscattered reactive differential cross section (corresponding to head-on reactive collisions). For resonance-coupling terms defined at large radial distances, high l values were preferred for reactions giving predominantly front scattering (which correspond to stripping-type reactive collisions).

The next level of approximation for the present model will be to introduce angularly dependent potentials and thus investigate the effects of coupling of internal and orbital angular momentum. Of considerable interest also will be the effectiveness of the resonance-coupling approximation in predicting cross sections for asymmetric systems involving product excitations.

*Work supported by the National Science Foundation and the Advanced Research Project Agency.

†Present address: Quantum Theory Project, Nuclear Sciences Building, University of Florida, Gainesville, Fla. 32610.

¹M. Karplus, R. N. Porter, and R. D. Sharma, *J. Chem. Phys.* **43**, 3259 (1965).

²D. A. Micha, *Arkiv Fysik* **30**, 411 (1965); **30**, 425 (1965); **30**, 437 (1965).

³M. Karplus, and K. T. Tang, *Discussions Faraday Soc.* **44**, 56 (1967).

⁴W. A. Lester, and R. B. Bernstein, *J. Chem. Phys.* **48**, 4896 (1968).

⁵S. Datz and E. H. Taylor, *J. Chem. Phys.* **39**, 1896 (1963).

⁶J. Geddes, H. F. Krause, and W. L. Fite, in *Abstracts of Papers to the Sixth International Conference on the Physics of Electronic and Atomic Collisions* (MIT Press, Cambridge, Mass., 1969), p. 635.

⁷H. Harrison, *J. Chem. Phys.* **37**, 1164 (1962).

⁸W. L. Fite, and R. T. Brackmann, in *Atomic Collision Processes*, edited by M. R. C. McDowell (North-Holland, Amsterdam, 1964), p. 955; *J. Chem. Phys.* **42**, 4057 (1962).

⁹L. Landau, *Physik Z. Sowjetunion* **2**, 46 (1932).

¹⁰C. Zener, *Proc. Roy. Soc. (London)* **A137**, 696 (1933).

¹¹S. Glasstone, K. J. Laidler, and H. Eyring, *Theory of Rate Processes* (McGraw-Hill, New York, 1941), p. 136.

¹²M. G. Evans and M. Polanyi, *Trans. Faraday Soc.* **34**, 11 (1938).

¹³S. Golden, *J. Chem. Phys.* **17**, 620 (1949).

¹⁴M. G. Evans and E. Warhurst, *Trans. Faraday Soc.* **35**, 593 (1938).

¹⁵L. Pauling and E. B. Wilson, *Introduction to Quantum Mechanics* (McGraw-Hill, New York, 1935), Chap. X.

¹⁶R. N. Porter and M. Karplus, *J. Chem. Phys.* **40**, 1105 (1964).

¹⁷K. T. Tang and M. Karplus, *J. Chem. Phys.* **49**, 1675 (1968).

¹⁸R. deVogelaere, *J. Res. Natl. Bur. Std.* **54**, 119 (1955).

¹⁹N. F. Mott and H. S. W. Massey, *The Theory of Atomic Collisions* (Oxford U. P., Oxford, England, 1965), Chap. 14.

²⁰R. G. Gordon, *J. Chem. Phys.* **51**, 14 (1969).

²¹L. Landau and E. M. Lifshitz, *Quantum Mechanics* (Pergamon, New York, 1965), p. 552.

²²W. A. Lester, *J. Computational Phys.* **3**, 322 (1968).

²³T. Y. Wu and T. Ohmura, *Quantum Theory of Scattering* (Prentice-Hall, Englewood Cliffs, N. J., 1962), Sec. W.

²⁴A. Kuppermann and J. M. White, *J. Chem. Phys.* **44**, 4352 (1966).

²⁵Reference 11, p. 210.

²⁶F. T. Smith, *Phys. Rev.* **118**, 349 (1960).

²⁷E. A. Morse and R. B. Bernstein, *J. Chem. Phys.* **37**, 2019 (1962).

²⁸J. Geddes, H. F. Krause, and W. L. Fite, *J. Chem. Phys.* **52**, 3296 (1970).

²⁹B. A. Ridley, W. R. Schulz, and D. J. LeRoy, *J. Chem. Phys.* **44**, 3344 (1966).